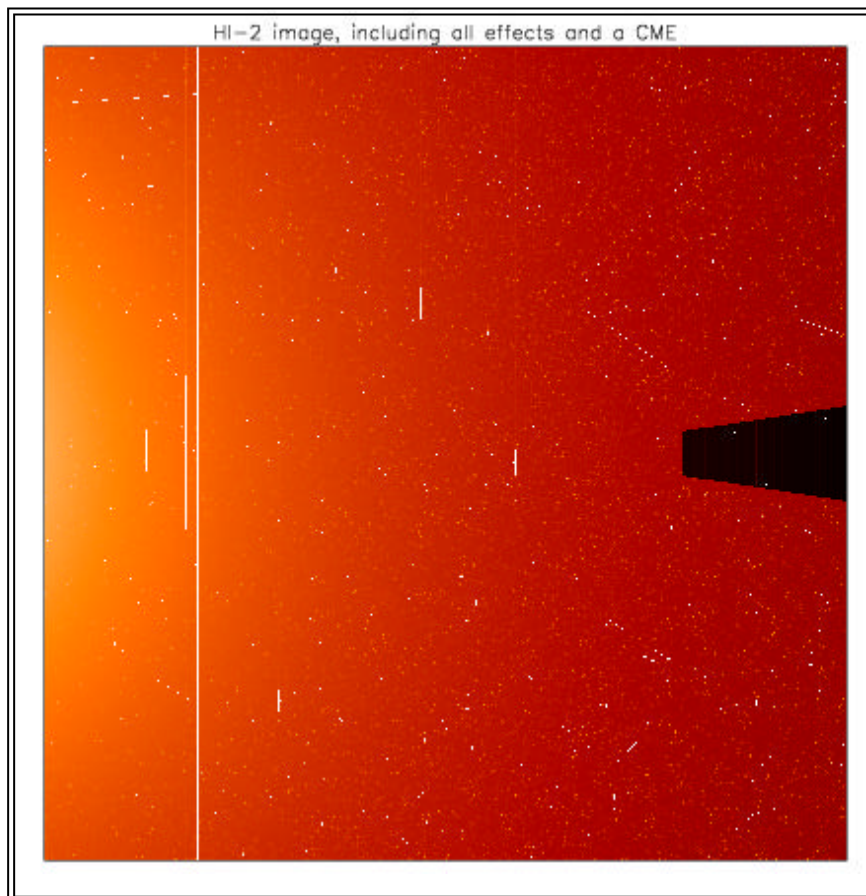


## Image Simulations for the Heliospheric Imager for the SECCHI /STEREO Project



Chris Davis  
Richard A. Harrison  
Space Science & Technology Department,  
Rutherford Appleton Laboratory,  
Chilton, Didcot, Oxfordshire OX11 0QX, UK  
[C.J.Davis@rl.ac.uk]

Version 3.4, 8 August 2003

## Contents

Version Sheet	Page 3
1. Introduction	Page 4
2. Relevant Documents	Page 4
3. Contributions to the HI Intensities	
3.1 F-Corona (zodiacal light)	Page 4
3.2 The Planets	Page 6
3.3 The Point Spread Function	Page 9
3.4 Stray Light	Page 9
3.5 Stars	Page 11
3.6 Noise	Page 13
3.7 Saturation and Blooming	Page 13
3.8 Line Transfer Exposures (non shutter operation)	Page 15
3.9 HI 2 Occulter	Page 18
3.10 Cosmic Rays	Page 19
4. A CME	Page 20
5. The 'Final Exposure'	Page 21
6. Exposure Sequences and Image Subtraction	Page 23
7. The IDL Code and the Next Steps	Page 28

## Version Sheet

Date	Version Number	Comments
13 November 2002	1	Initial draft
2 December 2002	1.1	Minor corrections
20 January 2003	2	Included cosmic rays, CME, image sequences & subtraction. Stars now to 12th magnitude.
13 June 2003	3.1	Cosmic ray correction made
22 July 2003	3.2	Cosmic ray tracks added
8 August 2003	3.4	HI 2 occulter added, significant optimisation carried out.

From version 3.1 onwards, the development of this code has been carried out by Chris Davis.

## 1. Introduction

This document describes the image simulation activity for the Heliospheric Imager (HI) aboard the NASA STEREO mission, using the HI\_SIM IDL code initiated by R. Harrison and subsequently developed by Chris Davis.

The HI\_SIM code is an attempt to include all contributions to the HI intensities as part of a facility to allow the investigation of CME identification and tracking, and to understand the intensity contributions for any pixel. It also allows the investigation of issues such as the size of the Earth-occultor, planetary saturation, and optimisation of exposure times. The code allows an analysis of HI-1 and HI-2 intensities with any desired exposure time.

## 2. Relevant Documents

The following documents provide inputs to the simulation or provide background information about HI.

- Ref. 1: HI-2 Design and Analysis document, CSL, issue dated 03/06/2002.
- Ref. 2: HI-1 Design and Analysis document, CSL, issue dated 18/02/2002.
- Ref. 3: Socker, D.G., Howard, R.A., Korendyke, C.M., Simnett, G.M. & Webb, D.F., Proc. of SPIE Vol. 4139, 284, 2000.
- Ref. 4: HI-1 Optical Design and Performances, TN/CSL/STE/01001, issue 2, 9 October 2001.
- Ref. 5: HI-2 Optical Design and Performances, TN/CSL/STE/01002, issue 2, 5 October 2001.
- Ref. 6: Derivation for the CCD Mask Occulter Dimensions Specification, Memo from T. Carter, 16 May 2003.

## 3. Contributions to the HI Intensities

### 3.1 F-corona (zodiacal light)

The intensity of the F-corona as a function of elongation, for both equatorial and polar directions, is given by refs. 1 and 2. It is calculated from the F-corona distribution given by Koutchmy and Lamy (1985). The equatorial values are roughly a factor of 2 brighter than the polar values. However, one would expect some variation in the F-coronal intensity, due to the nature of the streamer structures projecting into the heliosphere.

In the current version of this analysis, we only use the equatorial values for the F-corona, i.e. the worst case with regard to the brightness. For later versions of the code, some spatial variations and polar values can be included.

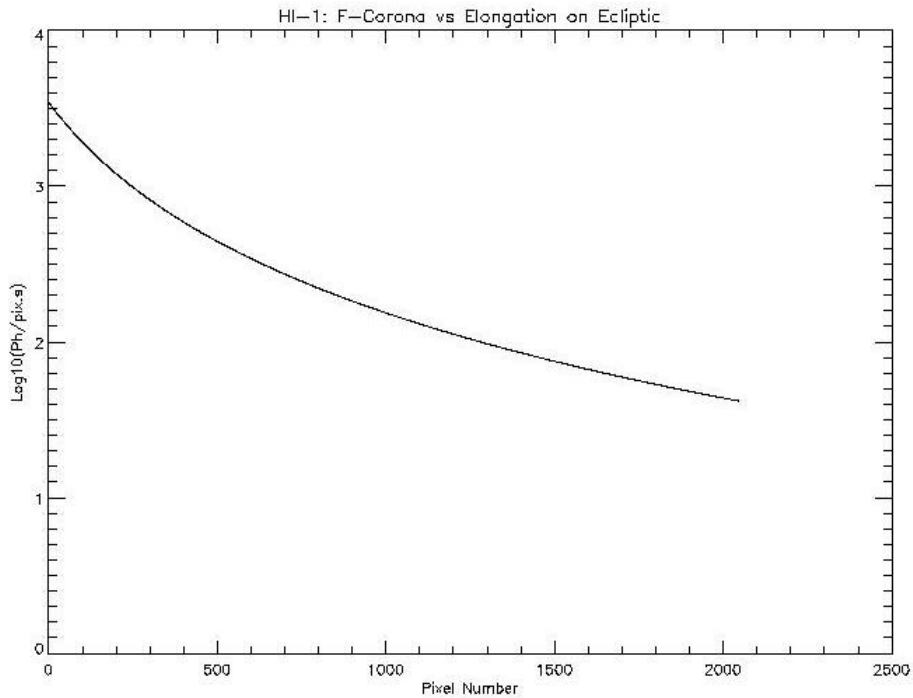


Fig. 3.1.1: The HI-1 F-corona intensity as a function of pixel number along the ecliptic.

The resulting F-coronal intensities in photons per pixel per second are given in Figs. 3.1.1 and 3.1.2. These are consistent with the relevant plots of refs. 1 and 2. Note that they are given for the 2048x2048 CCD array. The CCD image is 2x2 binned at a later stage, but we retain the full 2kx2k array at this time. The abscissa is given as pixel number (along the ecliptic line).

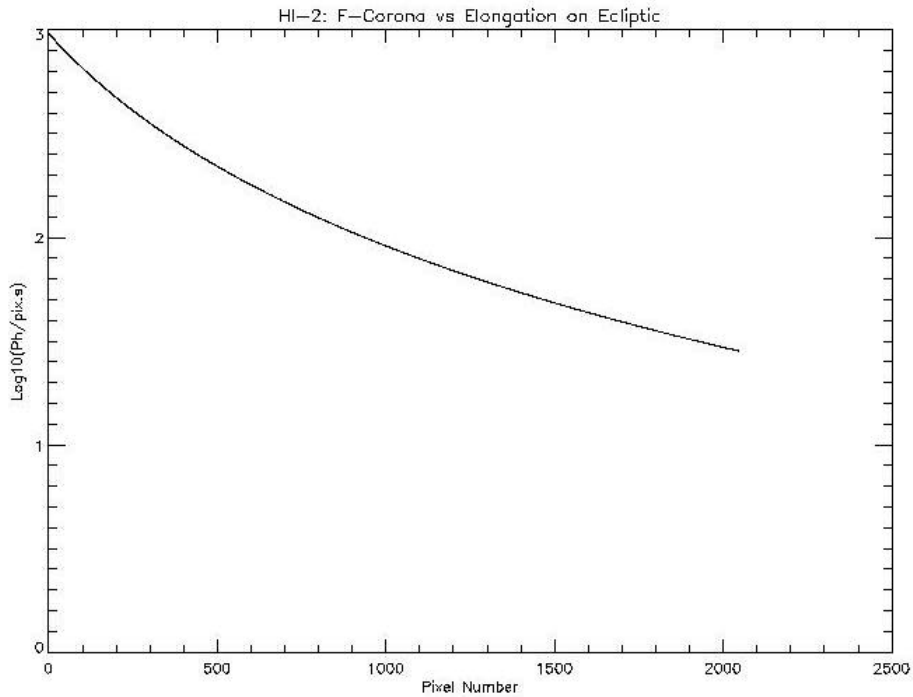
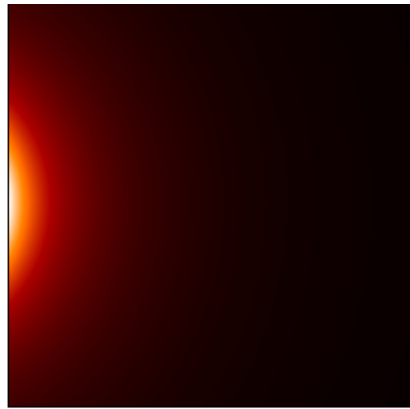


Fig. 3.1.2: The HI-2 F-corona intensity as a function of pixel number along the ecliptic.

The F-coronal distribution is assumed to be rotationally invariant (about Sun centre) for the simulation calculations at this time. The 2-D model of the F-corona used in the HI\_SIM analysis is shown, for HI-2 in Fig. 3.1.3.



*Fig. 3.1.3: The 2-D model distribution of the F-corona used for the HI-2 field of view.*

We note here that although the HI-1 and HI-2 fields of view are usually shown as circular in shape, we can in fact obtain data from the full area of the CCD. The optical quality of the corners may be poorer than the circular field, but may contain useful information. Thus, we do not restrict the analysis to the circular fields in the HI\_SIM code.

### 3.2 The Planets

The second stage of the analysis introduces the four planets Mercury, Venus, Jupiter and Mars. For the sake of calculation, we include all four planets in each field simulated, i.e. for HI-1 and HI-2. We also assume that each planet is at its brightest magnitude. Having all four bright planets in one HI-1 or HI-2 field would be rare and having all four at their maximum brightness values at the same time would be very unlikely, if not impossible. However, this extreme situation is used to simulate the worst case condition.

The planets are added at specific locations on or near the ecliptic. Specifically, using the 2048x2048 array, with (0,0) located at the bottom left and the ecliptic along the line  $y = 1024$ ,  $x = 0$  to 2047, we add Mercury at (360, 1024), Venus at (390,1050), Mars at (1200, 1000) and Jupiter at (1900,1024). The same co-ordinates are used for HI-1 and HI-2 simulations for ease of calculation.

The planets and stars are point sources, which are added to the HI fields of view. The table below shows the maximum magnitude of the planets and the brightness relative to the Sun of the planets and some stars. To obtain the count-rate in photons per second for a point source in HI-1 or HI-2 we use the figures given below:

Solar Constant [C]	1372 Wm <sup>-2</sup>
HI -1 collecting area (16 mm diam) [A]	2 x 10 <sup>-4</sup> m <sup>2</sup>
HI -2 collecting area (7 mm diam) [A]	4 x 10 <sup>-5</sup> m <sup>2</sup>
Detector Quantum Eff. assumed [DQE]	0.9
Fraction of black body curve [bb]	0.1 (HI -1) and 0.64 (HI -2)
Mean photon energy (HI -1) [E]	2.92 x 10 <sup>-19</sup> J (680 nm)
Mean photon energy (HI -2) [E]	3.31 x 10 <sup>-19</sup> J (600 nm)
Solar Image area (HI -1) [pix]	2076 (35 arcsec pixels, i.e. 2kx2k array)
Solar Image area (HI -2) [pix]	176 (2 arcmin pixels, i.e. 2kx2k array)
Solar Intensity (Bo) = [C.A.DQE.bb/E]	HI -1: 8.46 x 10 <sup>16</sup> ph.s <sup>-1</sup> HI -2: 9.55 x 10 <sup>16</sup> ph.s <sup>-1</sup>
Solar Intensity per pixel = [C.A.DQE.bb/E.pix]	HI -1: 4.08 x 10 <sup>13</sup> ph.s <sup>-1</sup> .pix <sup>-1</sup> . HI -2: 5.43 x 10 <sup>14</sup> ph.s <sup>-1</sup> .pix <sup>-1</sup> .

The planetary intensities listed are the maximum intensities viewed from Earth. Since the STEREO spacecraft are in 1 AU solar orbits, the same values apply.

The differences in the fraction of the black body curve detected by HI-1 and HI-2, combined with the different collecting areas, almost cancel out, resulting in very similar intensities in HI-1 and HI-2 for the planets and stars. Thus, for the purposes of the simulation, we take the HI-2 values for both simulations. For the purposes of this simulation, this is perfectly adequate.

Object	Max Magnitude (m)	Brightness (B = 10 <sup>(-m/2.5)</sup> )	B/Bo (Bo = 5.25x10 <sup>10</sup> )	HI -1 Ph/sec	HI -2 Ph/sec
Sun	-26.8	5.25 x 10 <sup>10</sup>	1	8.46 x 10 <sup>16</sup>	9.55 x 10 <sup>16</sup>
Venus	-4.6	69.2	1.3 x 10 <sup>-9</sup>	1.10 x 10 <sup>8</sup>	1.24 x 10 <sup>8</sup>
Jupiter	-2.6	11	2.1 x 10 <sup>-10</sup>	1.78 x 10 <sup>7</sup>	2.00 x 10 <sup>7</sup>
Mercury	-1.8	5.2	9.9 x 10 <sup>-11</sup>	8.38 x 10 <sup>6</sup>	9.45 x 10 <sup>6</sup>
Mars	-1.6	4.4	8.4 x 10 <sup>-11</sup>	7.11 x 10 <sup>6</sup>	8.02 x 10 <sup>6</sup>
Sirius	-1.47	3.9	7.4 x 10 <sup>-11</sup>	6.26 x 10 <sup>6</sup>	7.07 x 10 <sup>6</sup>
Arcturus	-0.06	1.1	2.1 x 10 <sup>-11</sup>	1.78 x 10 <sup>6</sup>	2.00 x 10 <sup>6</sup>
Rigil	0	1	1.9 x 10 <sup>-11</sup>	1.61 x 10 <sup>6</sup>	1.81 x 10 <sup>6</sup>
Mag 1.0	1	0.4	7.6 x 10 <sup>-12</sup>	6.43 x 10 <sup>5</sup>	7.26 x 10 <sup>5</sup>
Mag 2.0	2	0.2	3.8 x 10 <sup>-12</sup>	3.21 x 10 <sup>5</sup>	3.63 x 10 <sup>5</sup>
Mag 3.0	3	0.06	1.1 x 10 <sup>-12</sup>	9.31 x 10 <sup>4</sup>	1.05 x 10 <sup>5</sup>
Mag 4.0	4	0.03	5.7 x 10 <sup>-13</sup>	4.82 x 10 <sup>4</sup>	5.44 x 10 <sup>4</sup>
Mag 5.0	5	0.01	1.9 x 10 <sup>-13</sup>	1.61 x 10 <sup>4</sup>	1.81 x 10 <sup>4</sup>
Mag 6.0	6	0.004	7.6 x 10 <sup>-14</sup>	6.43 x 10 <sup>3</sup>	7.27 x 10 <sup>3</sup>
Mag 7.0	7	0.0016	3.0 x 10 <sup>-14</sup>	2.54 x 10 <sup>3</sup>	2.87 x 10 <sup>3</sup>
Mag 8.0	8	0.00063	1.2 x 10 <sup>-14</sup>	1.02 x 10 <sup>3</sup>	1.15 x 10 <sup>3</sup>
Mag 9.0	9	0.00025	4.8 x 10 <sup>-15</sup>	4.06 x 10 <sup>2</sup>	4.59 x 10 <sup>2</sup>
Mag 10.0	10	0.00010	1.9 x 10 <sup>-15</sup>	1.61 x 10 <sup>2</sup>	1.82 x 10 <sup>2</sup>
Mag 11.0	11	0.00004	7.6 x 10 <sup>-16</sup>	6.43 x 10 <sup>1</sup>	7.27 x 10 <sup>1</sup>
Mag 12.0	12	0.000016	3.0 x 10 <sup>-16</sup>	2.54 x 10 <sup>1</sup>	2.87 x 10 <sup>1</sup>

Planetary and stellar saturation and blooming are discussed below. However, for nominal exposures - 12 s for HI-1 and 60 s for HI-2, the intensities shown in red will saturate.

Fig. 3.2.1 shows a plot of intensity along the ecliptic ( $y=1024$ ), which displays the F-corona, and Mercury and Jupiter, which were placed right on the ecliptic.

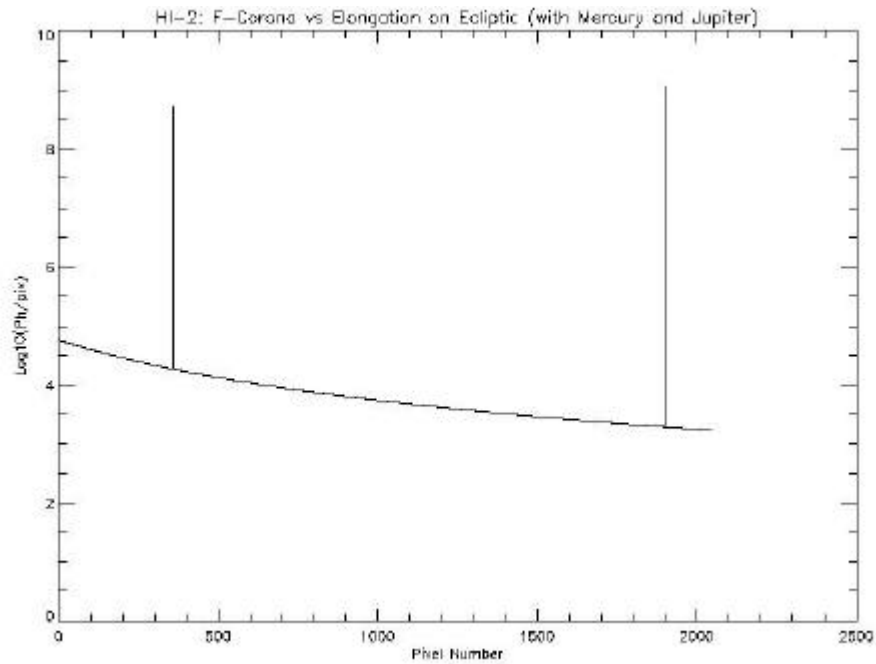


Fig. 3.2.1: A plot of intensity vs elongation, or pixel number, including Mercury (left) and Jupiter (right), in this case, for HI-2 with a 60 s exposure.

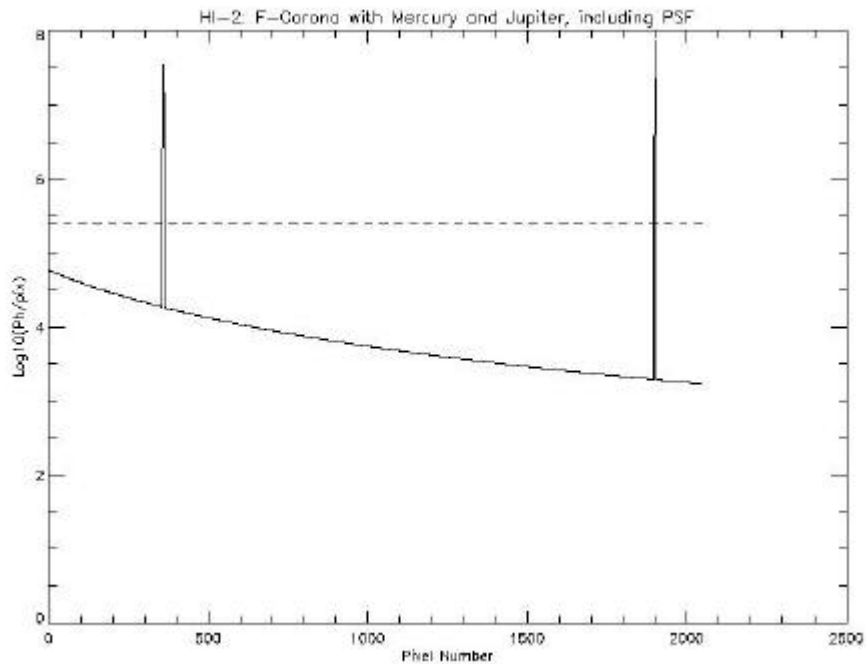


Fig. 3.3.1: The same plot as Fig. 3.2.1 but with the PSF applied to the data.

### 3.3 The Point Spread Function

Optical modelling performed by CSL (refs. 4 and 5) shows that the HI-1 and HI-2 RMS size for a point source is of order 50  $\mu\text{m}$  and 100  $\mu\text{m}$  in the worst case, respectively (see Fig. 6 of Ref 4 and Fig. 7 of ref. 5). Note that the pixel size is 13.5  $\mu\text{m}$ . Calculations show that of order 34 % of the spot energy is in the central pixel and this information, along with the RMS value, is used to model a basic Gaussian shaped point spread function.

Fig. 3.3.1 shows the same plot as Fig. 3.2.1 with the point spread function (PSF) applied. The PSF is applied to the four planets, and is (later) applied to all stars introduced to the field. Fig. 3.3.1 also shows the saturation level. The pixels saturate at 200,000 electrons, i.e. 200,000/DQE photons. At a DQE of about 80 %, this gives a value at 250,000 photons or  $\log(\text{Ph}/\text{pix}) = 5.4$ . Clearly, the two planets will saturate.

### 3.4 Stray Light

To mimic the stray light of the instrument, the CSL measurements of the forward baffle optical model are used (May 2002) including a  $10^{-4}$  rejection from the telescope assembly. These measurements are shown in Fig. 3.4.1.

Although the HI-1 and HI-2 angular off-sets from a Sun-centred bore-sight are 3.65-23.65 degrees and 18.35-88.35 degrees, respectively, the stray light contributions to each field are not to be read-off Fig. 3.4.1 for those angular ranges. The relevant stray-light angular range to consider for HI-1 is from 1.5-3.3 degrees. This is the range for which the rays diffracted by the front baffle scatter into the optical system, but are not part of the HI-1 field of view, i.e. this range is the brightest shadow region passing into the HI-1 field. As can be seen from the figure, that gives the range  $10^{-8}$  to  $2 \times 10^{-11}$ . With the  $10^{-4}$  rejection of the lens assembly, that provides a total of  $10^{-12}$  to  $2 \times 10^{-15}$  across the HI-1 field.

Similarly, for HI-2, the rejection from the front baffle is of order  $6 \times 10^{-12}$ , giving a total of  $6 \times 10^{-16}$  of the solar intensity. For HI-2, this is effectively flat across the elongation range. Thus, for HI-2, we convert this to  $\text{ph}\cdot\text{pix}^{-1}\cdot\text{s}^{-1}$  using the solar intensity in the table of section 3.2 ( $5.43 \times 10^{14} \text{ ph}\cdot\text{s}^{-1}\cdot\text{pix}^{-1}$ ). This gives a stray light intensity per pixel at  $0.33 \text{ ph}\cdot\text{pix}^{-1}\cdot\text{s}^{-1}$ .

For HI-1, the effect is very different. To mimic the stray light measurements of CSL, the function  $(6 \times 10^{-16}) + (4 \times 10^{-12} \times e^{-(\text{pix}/70)})$  is used, where  $\text{pix}$  is the distance from the location (0, 1024). The intensity is scaled to  $\text{ph}\cdot\text{pix}^{-1}\cdot\text{s}^{-1}$  using the factor  $4.08 \times 10^{13}$  (section 3.2). This gives a stray-light contribution from  $40.8 \text{ ph}\cdot\text{pix}^{-1}\cdot\text{s}^{-1}$  at (0,1024) to  $0.08 \text{ ph}\cdot\text{pix}^{-1}\cdot\text{s}^{-1}$  at (2047,1024).

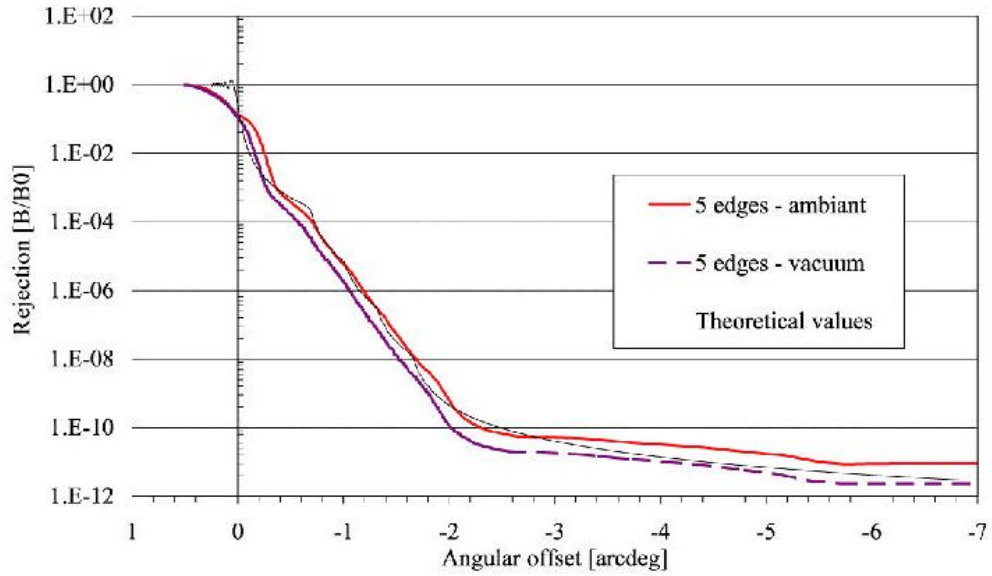


Fig. 3.4.1: The CSL stray light measurements of the forward baffle mock-up (May 2002). To obtain the full light rejection performance, a figure of about  $10^{-4}$  must be included for the lens barrel assemblies.

Fig. 3.4.2 shows the expected stray light as a function of pixel along the ecliptic line (from (0,1024) to (2047,1024)), for both HI-1 and HI-2 on the same plot.

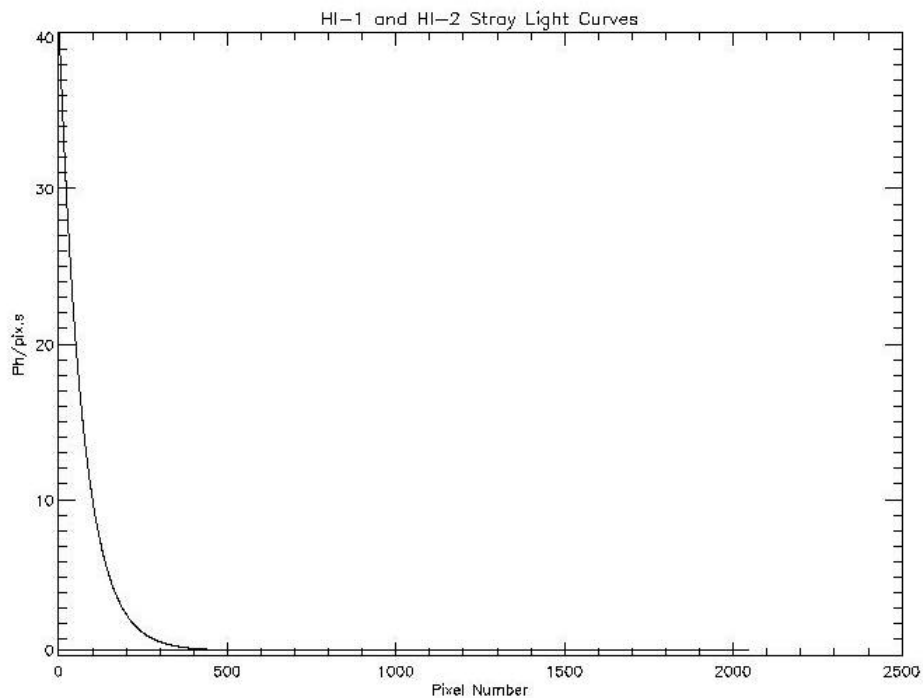


Fig. 3.4.2: The stray light model used for the HI\_SIM analysis for HI-1 (range 40.8 to 0.08) and HI-2 (0.33). For each instrument, the stray light contribution is plotted vs pixel number along the ecliptic line.

### 3.5 Stars

We require a distribution of point sources to mimic the stellar distribution. The approximate number of stars per square degree, as a function of magnitude has been published (e.g. Allen, C.W., *Astrophys. Quantities*, Athlone Press) and we make use of this, projecting to the size of the HI fields of view. We do include a few stars of magnitude brighter than 0.0 in each calculation, which would be rather unusual, but is required to estimate the worst case situation. Thus, for both HI-1 and HI-2 we assume the inclusion of Sirius, Arcturus and Rigil, and for each magnitude considered we assume at least one star in the field of view.

The stellar magnitudes and intensities are included in the table in section 3.2. Below, we show the anticipated stellar distribution for the HI fields of view.

Each star is added to the field of the modelled image at a location estimated using an IDL random number generator. The PSF is applied to each star. Note that in section 3.2, the stellar intensities were estimated and those liable to saturate the pixels were highlighted. The distribution of intensities shown in that table shows that this is for relatively few stars.

Mag	No. in HI -1 field	No. in HI -2 field
-1.47 (Sirius)	1	1
-0.06 (Arcturus)	1	1
0.0 (Rigil)	1	1
1.0	1	1
2.0	1	4
3.0	1	14
4.0	4	48
5.0	13	150
6.0	39	450
7.0	109	1335
8.0	314	3848
9.0	884	10843
10.0	2552	31277
11.0	6867	84156
12.0	18068	221414

Figs. 3.5.1 and 3.5.2, using the same format as Fig. 3.3.1, but with a number of near-ecliptic strips, show many stars in addition to Mercury and Jupiter, for HI-1 and HI-2. These simulations used stellar magnitudes down to 10, though the code allows simulations including stars to 12th magnitude.

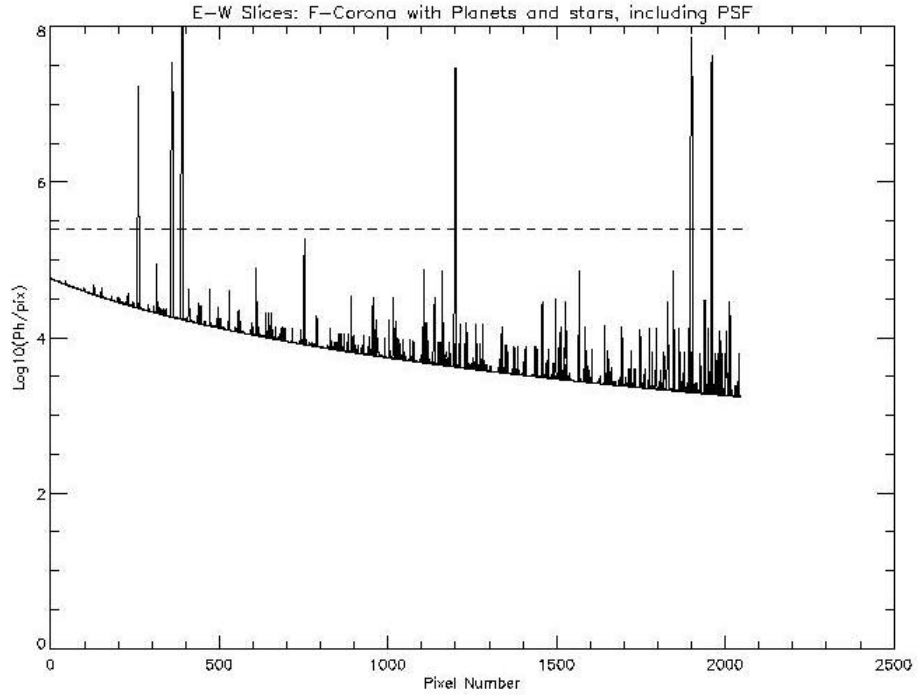


Fig. 3.5.1: HI-2 intensity vs elongation plots shown for a number of rows near the ecliptic plane superimposed on the same plot. Specifically, the intensities for rows  $y = 1024$  (ecliptic), 980, 1000, 1030, 1050 are shown. The exposure time is 60 s and stars to  $10^{\text{th}}$  magnitude are included.

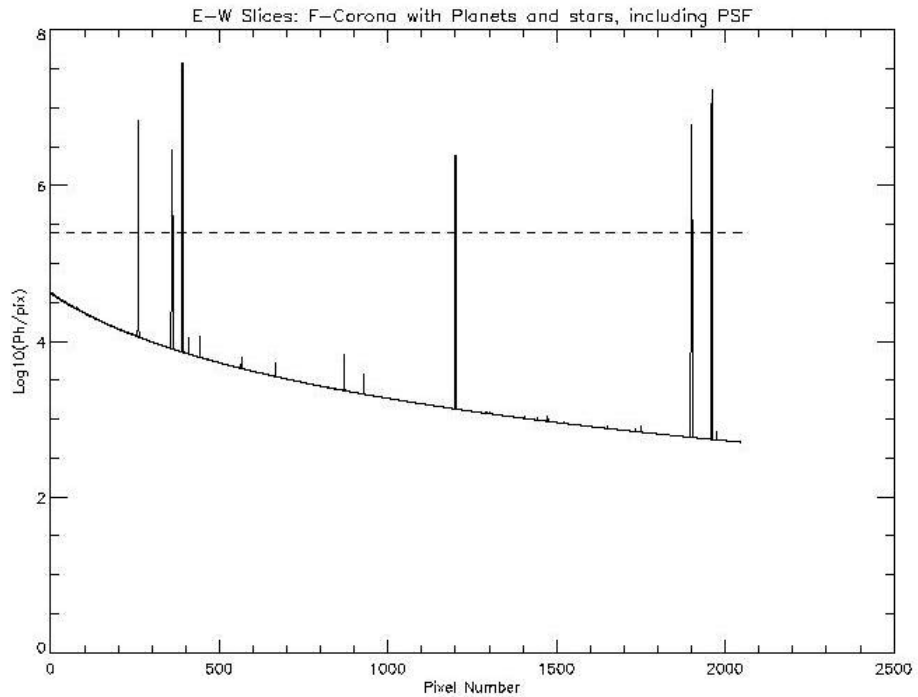


Fig. 3.5.2: HI-1 intensity vs elongation plots shown for a number of rows near the ecliptic plane superimposed on the same plot. Specifically, the intensities for rows  $y = 1024$  (ecliptic), 980, 1000, 1030, 1050 are shown. The exposure time is 12 s and stars to  $10^{\text{th}}$  magnitude are included.

### 3.6 Noise

Noise is now included, assuming a Poisson-like form. Using the IDL 'randomn' function (mean value 0.0 with standard deviation of 1.0), each pixel intensity,  $I$ , is modified using the following form:

$$I = I + \text{sqrt}(I \times \text{randomn}(\text{seed})).$$

This is a simple-minded yet effective approach for the modelling effort. The result of this calculation is shown in Figs. 3.7.1 and 3.7.2, which show the same data as Fig. 3.5.1 including noise (and blooming – see next section).

### 3.7 Saturation and Blooming

As noted in section 3.3, pixels saturate at 200,000 electrons, i.e. 200,000/DQE photons. At a detector QE of about 80 %, this gives a value at 250,000 photons or  $\log(\text{Ph}/\text{pix}) = 5.4$ .

When a pixel saturates, we assume that charge is 'spilled' or distributed along the column, rather than along rows (across columns). Cross-column saturation is subdued by the detector design. The level to which saturation can be confined to columns has to be confirmed with detector tests, though initial tests are encouraging. Thus, in the HI\_SIM code, each pixel intensity is capped at 250,000 photons, and excess intensity is spread symmetrically along the column. In the current version of the code, there is no lateral spread.

Figs. 3.7.1 and 3.7.2 show the same data as Figs. 3.5.1 and 3.5.2 with the saturation level imposed and the excess intensity spread as described, and Fig. 3.7.3 shows part of an HI-2 image with the blooming included.

Note that the PSF is applied prior to the saturation, i.e. a star's intensity will be spread (using a Gaussian form) across a number of pixels, and it is the resulting intensities which, if they saturate, will show blooming. Thus, a bright star will show saturation along a few adjacent columns despite the fact that we have subdued cross-column blooming.

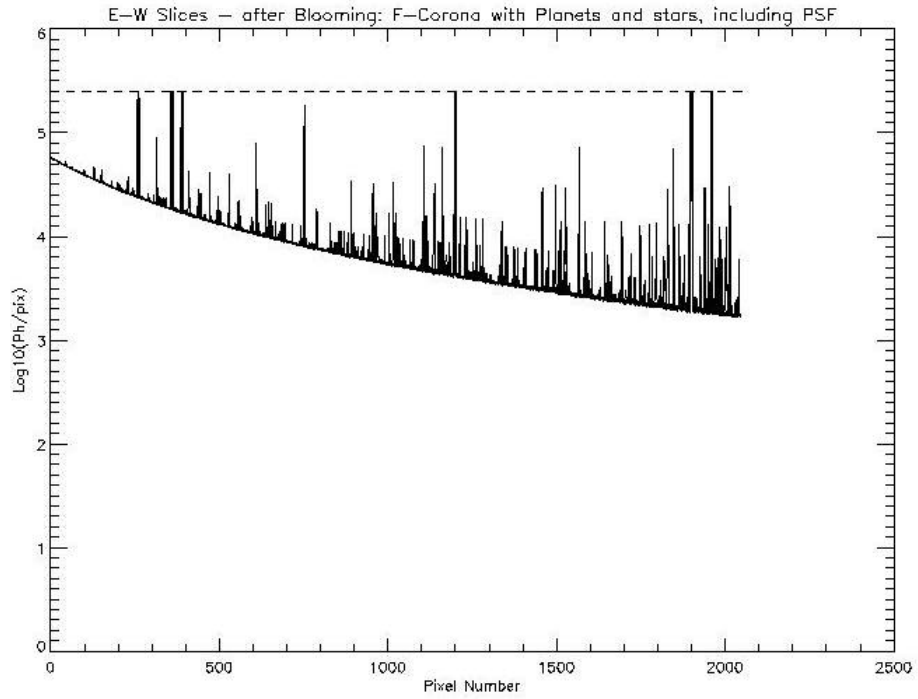


Fig. 3.7.1: The same as Figure 3.5.1 including noise and the saturation limit.

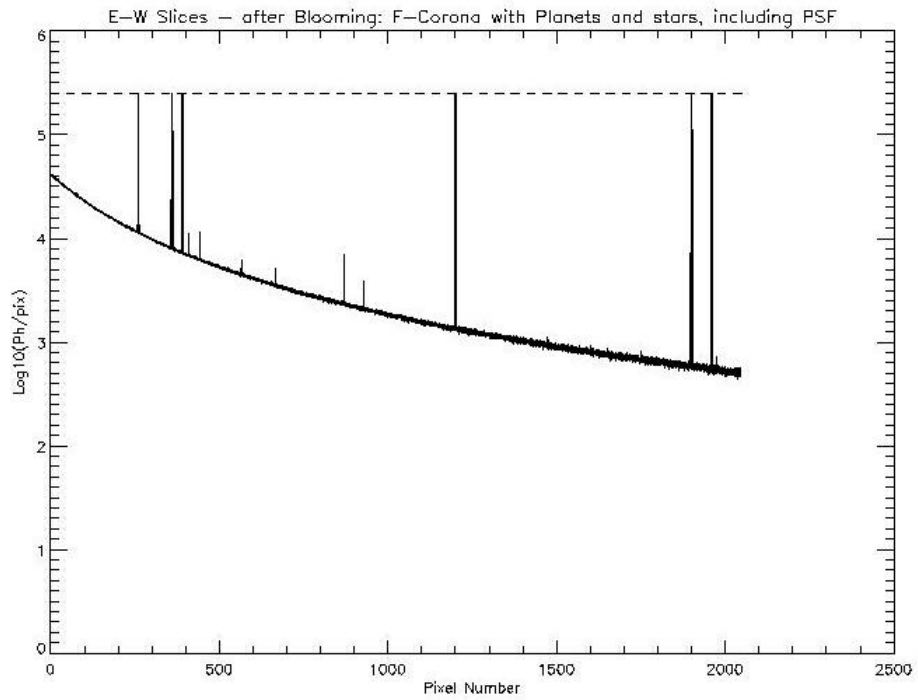


Fig. 3.7.2: The same as Figure 3.5.2 including noise and the saturation limit.

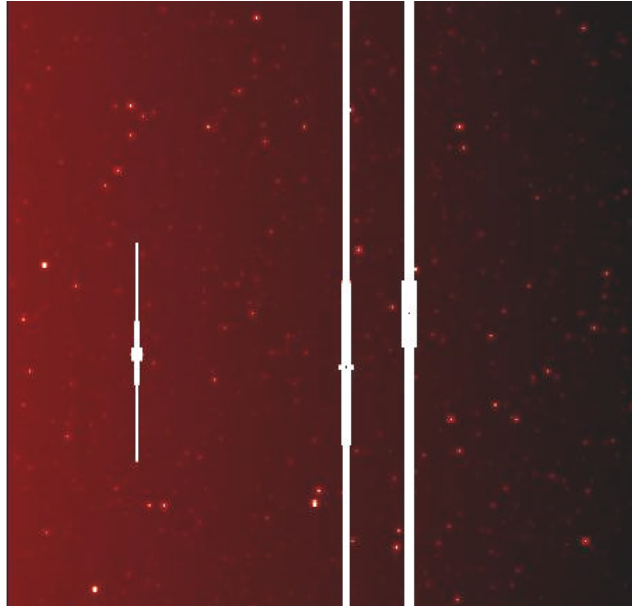


Fig. 3.7.3: A partial HI -2 image showing the blooming of some sources. The region covered is  $x = 200-500$ ,  $y = 900-1200$ .

### 3.8 Line Transfer Exposures (non-shutter operation)

The HI instrument does not have a shutter facility. The consequences of this are shown schematically in Fig. 3.8.1.

Let us examine pixel  $(n,m)$  of the exposed image, and an exposure time of  $N$  seconds. The read-out direction of the CCD is downwards and the line transfer rate is  $2048 \mu\text{s}$ , resulting in a 'pseudo exposure' at every line position along the column under the pixel location. In other words in addition to the nominal exposure, there are  $(m-1)$  exposures of  $2048 \mu\text{s}$ , which must be added to the nominal exposure intensity because there is no shutter.

In addition, the CCD is cleared using a  $150 \mu\text{s}$  line transfer rate, so we must also add contributions from the  $(2048-m)$  pixels above the nominal location with an exposure of  $150 \mu\text{s}$  at each location.

In mathematical form, the total count,  $T$ , you will read out for pixel  $(n,m)$  is given by:

$$T(n,m) = [N \times I(n,m)] + \sum_{(y=m+1,2047)} (150 \times 10^{-6}) \times I(n,y) + \sum_{(y=0,m-1)} (2048 \times 10^{-6}) \times I(n,y)$$

where the count rate for pixel  $(x,y)$  is given by  $I(x,y)$ .

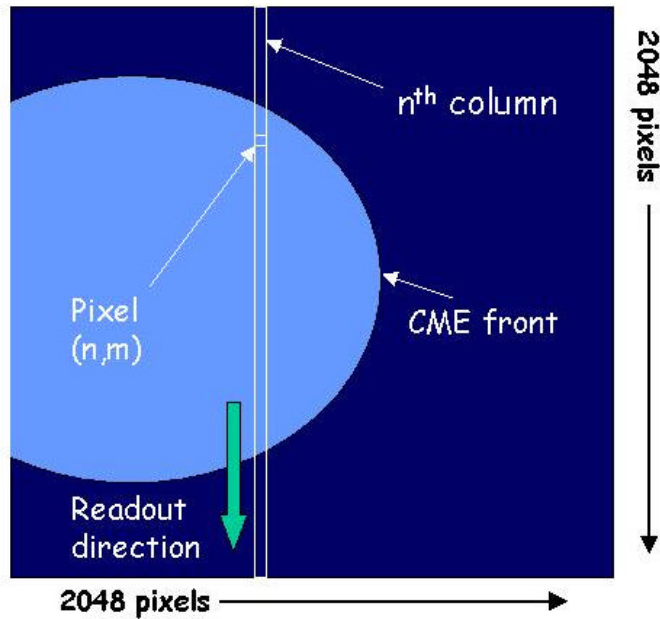


Fig. 3.8.1: A schematic display of the non-shutter read out. For details, see text.

The HI\_SIM code includes the non-shutter contribution and thus allows an investigation of its impact. Fig. 3.8.2 shows the intensity distribution along the central column,  $x = 1024$  from  $y = 0$  to 2047. The upper curve shows the F-coronal distribution plus the planets and stars. The lower curve shows the same assuming a shutter. One can readily see the effect, i.e. an increase in the contribution from the 2048  $\mu$ s pseudo exposures for larger values of  $y$ .

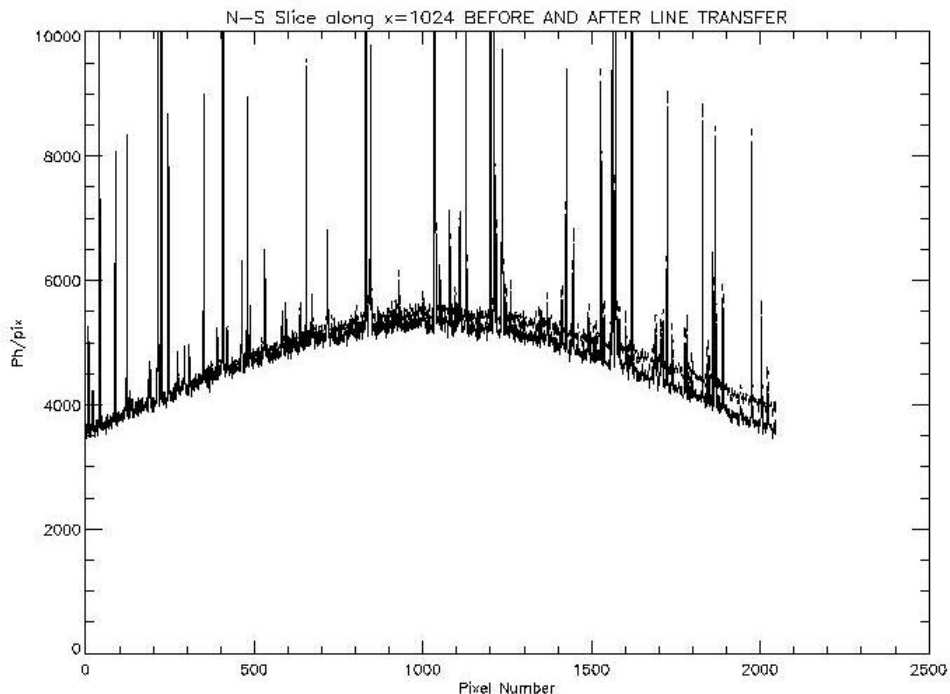
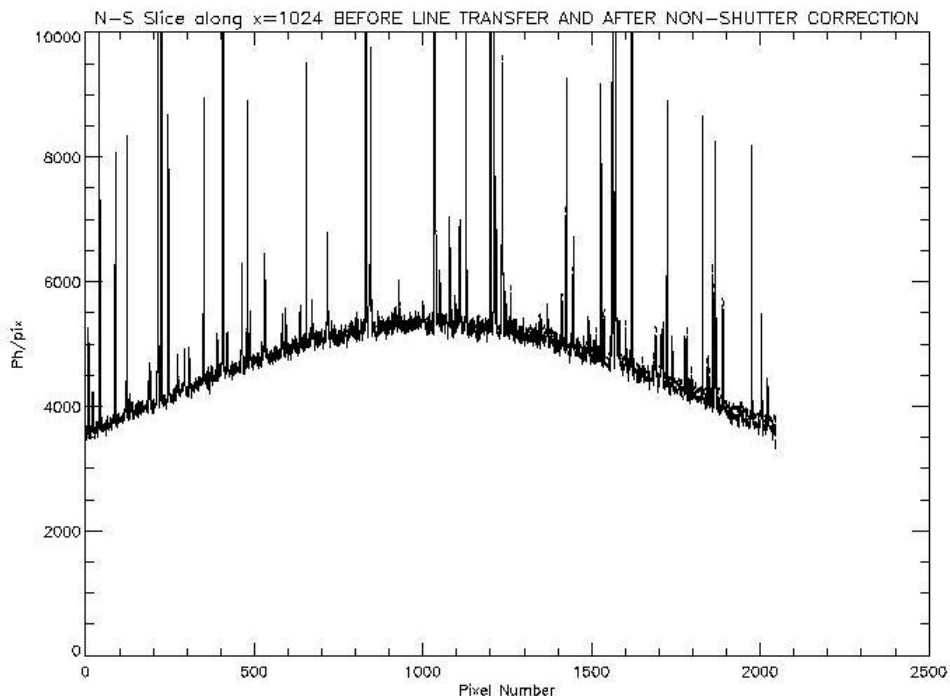


Fig. 3.8.2: A comparison of the intensities along the  $x = 1024$  column (solar north is to the right) for a shutter operation (lower curve) and non-shutter operation (upper curve), for a 60 s exposure including stars down to  $10^{\text{th}}$  magnitude.

Note that although there are stars (down to  $10^{\text{th}}$  magnitude in the example) in this analysis, the difference between the 60 s exposure and the 2048  $\mu\text{s}$  exposure (factor of 29,297) means that most stars produce an insignificant step function in the curves of Fig. 3.8.2. In principle, a very bright source, exposed at 2048  $\mu\text{s}$  could produce a bright vertical 'streak' for all pixels in the same column, above the source. We discuss the impact of this effect later.

Thus, the basic shape of the underlying curve of Fig. 3.8.2 is in effect a gradient determined by the number of pixels contributing to the 2048  $\mu\text{s}$  pseudo exposures of each pixel. This is a gradient which is known, and it can be used to 'correct' for the non-shutter exposures. This is done in a most basic sense in Fig. 3.8.3. The gradient is calculated using an averaging routine (to ensure that the effects of noise are not magnified), and one can see that the 'corrected' curve is very close to the original. It must be noted that this is a first attempt at such a correction and far more sophisticated methods may be employed. It is shown here to demonstrate that the non-shutter operation is feasible and has little if any impact on the scientific return of HI. The previous version of the code contained a bug whereby the noise was not added to the pre-non-shutter exposure. As a result, noise was not propagated through the correction procedure. This has now been included in the code, and although it alters the results very slightly, makes no difference to the conclusion that non-shutter operations are feasible.



*Fig. 3.8.3.: The same as Fig. 3.8.2. but the non-shutter curve has been corrected, as discussed in the text, using an average gradient technique. The non-shutter curve is now much closer to the shutter curve.*

### 3.9 The HI 2 Occulter

The HI instruments are designed to view the Sun-Earth line and in the early days of the mission, with the spacecraft closest to the Earth, the intensities of the Earth and Moon in the HI 2 instrument will be so large that they would saturate large sections of the CCD. In order to prevent this, a mask has been designed for the HI 2 instrument that will block light from the Earth and Moon until the spacecraft have move sufficiently far from the Earth that the intensities of the planet will be no greater than that of Venus (see, for example the memorandum from Tim Carter 'Derivation for the CCD Mask Occulter Dimensions Specification' on May 16 2003).

The shape of the occulter has been carefully designed to account for the expected tolerances in the pointing accuracy of the spacecraft while minimising the area of the CCD that is obscured. As the mission evolves and the spacecraft move away from the Earth along the Earth's orbital path, the image of the Earth and Moon will decrease in size and drift inwards from the right hand side of the HI 2 image. The occulter is therefore a rhomboid extending 5.67mm (420 pixels) in length over the central right-hand edge of the CCD array, tapering from a width of 3.24mm (240 pixels) at the CCD edge to a width of 1.5mm (111 pixels) at the tip.

The occulter will prevent any light from the optics reaching selected areas of the CCD but will not stop cosmic rays or saturation spill-over from neighbouring pixels from charging the underlying pixels.

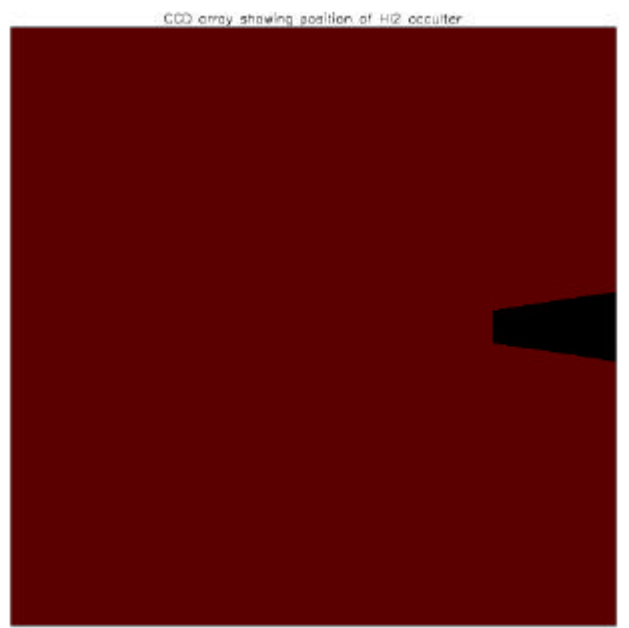


*Fig 3.9.1, HI 2 occulter is a rhombic shape overlying the central right-hand edge of the CCD array*

In this simulation, a byte-mask (an array of zeros and ones) is defined which represents the CCD array. All values within this byte-mask are set to 1 except those values corresponding to pixels under the occulter which are set to zero. Multiplying the simulated intensities in the CCD by the numbers this array, automatically sets those values beneath the occulter to zero. The effects of cosmic rays, noise, and pixel saturation can then be applied subsequently, allowing for the possibility that some pixels under the occulter may be charged by such processes.

In the final images, the occulter appears as a dark area on the central right-hand side of the image.

### 3.10 Cosmic Rays

Cosmic rays are added in random locations assuming a similar rate to those detected by the CDS instrument on SOHO (Pike and Harrison, 2000, A&A 362, L21). Thus, we assume  $4 \text{ hits.cm}^{-2}\text{s}^{-1}$  (this was overestimated in the previous version of this document by a factor of ten. The following calculations have now been changed to account for this error). We have a  $2048 \times 2048$  array of 13.5 micron pixels, i.e.  $2.76 \text{ cm} \times 2.76 \text{ cm}$ , which suggests 30.5 hits per second on each of the HI CCDs. In principle, cosmic ray hits can be point-like (single pixel), can spill into adjacent pixels or even be tracks. In addition, the intensity of a cosmic ray hit may vary. In the previous version of this code, cosmic ray hits were simulated as being point-like sources that saturated the pixel. This code includes the effects of cosmic ray tracks. Cosmic rays are assumed to arrive from any direction in a uniform distribution and saturate all pixels of the CCD that they pass through (250000 counts). Since the active depth of the CCD pixels is only of the order of 10 microns, it is very unlikely that many cosmic ray tracks of any significant length will be seen within the HI instruments.

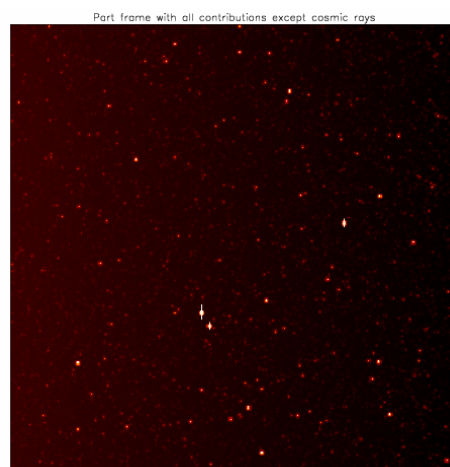


*Fig. 3.10.1: An area of the HI-2 simulated field, for a single 60 s exposure, including the F-corona, scattered light, stars to 12th magnitude, planets, the point spread function, noise and the non-shutter read out effect. The area is 400 x 400 pixels.*

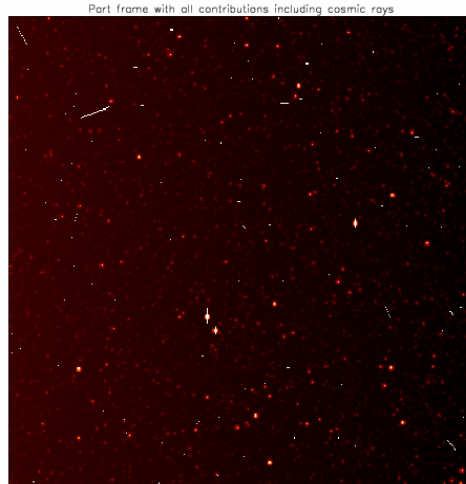


Fig. 3.10.2: The same simulated image as Fig. 3.10.1. but with cosmic rays

To put the particle hit rate in perspective, note that for a 60 s exposure, we expect 1,830 pixels hits out of the 4,194,304 pixels, i.e. 0.04 % of pixels are effected. Note that the HI operation will usually consist of sequences of exposures added together prior to telemetering to the ground. The accumulated exposure time of a returned image may be 1 hour. For a single exposure of 1 hour, approximately 2.6% of all pixels in the image would be contaminated by cosmic rays. This may not be acceptable. Thus, whilst the on-board image summing allows us to return 32 bit pixels, rather than the 16 bits returned from the camera (to achieve count rates with noise levels appropriate for our needs), it also allows us to clean each exposure prior to summing, to minimise the impact of the cosmic rays.

Figs. 3.10.1 and 3.10.2 show an area of the HI-2 field with all effects included. The only difference is the fact that Fig. 3.10.2 includes cosmic ray hits.

#### **4. A CME**

Finally, we add the simulated CME, i.e. the feature which must be identified and analysed despite the effects of the phenomena considered above.

For this, we take a simple semi-circle centred on location (0,1024), with radius 605 pixels and thickness 11 pixels. The intensity is taken from Socker et al. (Ref. 3). For HI-1 the intensity is given as  $10^{-13}$  Bo. Socker et al. suggest that the range across the HI-1 field should be from  $10^{-12}$  to  $10^{-14}$  Bo. Similarly, for HI-2, the expected range is  $10^{-14}$  to  $3 \times 10^{-16}$  and we take  $10^{-15}$  Bo. Bo itself is of order  $10^{17}$  ph.s<sup>-1</sup>.

The CME location is shown in Fig. 4.1. However, this is for display purposes; the actual intensity is much less than the F-coronal intensity. In a single exposure, the CME intensity level is weaker than the noise level on the F-coronal intensity.

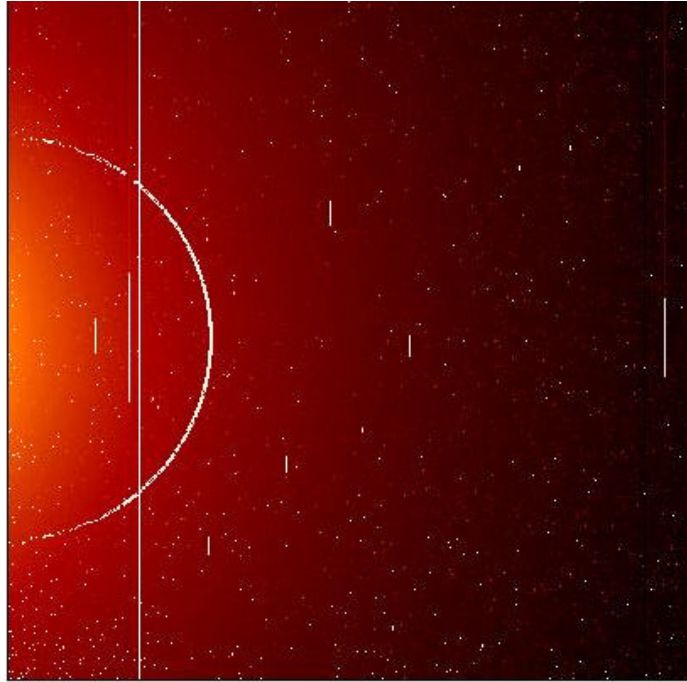


*Fig. 4.1: The dummy CME-loop. This frame is included to show the CME location. The CME intensity has been increased to saturation levels for this, but would normally be about two orders of magnitude weaker than the F-corona.*

## 5. The 'Final Exposure'

Figs. 5.1 and 5.2 show HI-1 and HI-2 frames modelled using the HI\_SIM codes and including all of the features discussed above, i.e. the F-corona, scattered light, stars to 12th magnitude, four planets (Venus, Jupiter, Mercury and Mars), the instrumental PSF, cosmic rays, the non-shutter read-out effect, noise, saturation and blooming and a dummy CME. Of course, in these single exposures, the CME intensity is impossible to readily identify. CMEs will be detected through exposure summing and differencing techniques, and this is discussed in the next section.

Note that the frames are still in 2048 x 2048 format and that the conversion to jpg format and insertion into a Word document have resulted in some degradation of the resolution. Nevertheless, they provide an accurate representation of the HI images. For high quality versions of the images see the UK STEREO Web site <http://www.stereo.rl.ac.uk/> and, under 'Documents' select either the HI-1 or HI-2 simulated image (postscript).

HI-1 image, including all effects and a CME

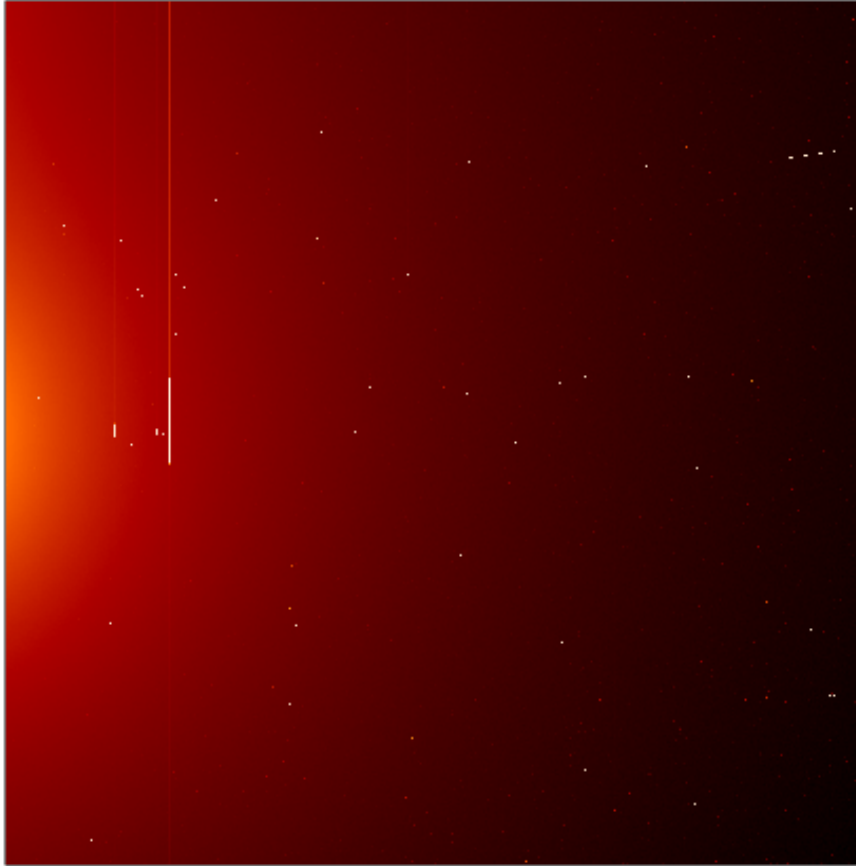


*Fig. 5.1: A simulated HI -1 12 s exposure (still in 2048x2048 format), including the F-corona, scattered light, stars to 12th magnitude, four planets (Venus, Jupiter, Mercury and Mars), the instrumental PSF, cosmic rays, the non-shutter read-out effect, noise, saturation and blooming and a dummy CME. Cosmic ray tracks can appear as dotted lines due to the reduced resolution of the images in this document. For higher resolution images, see the online postscript files.*

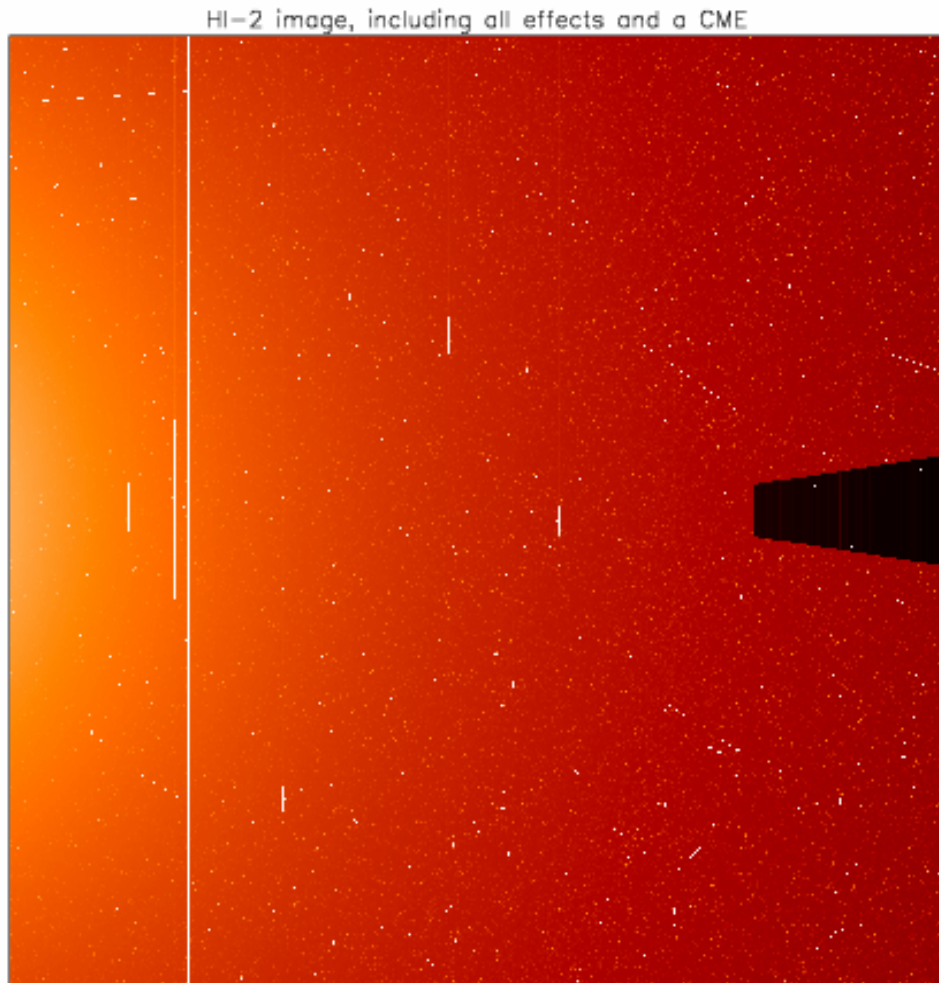


*Fig. 5.2: A simulated HI-2 60 s exposure (still in 2048x2048 format), including the F-corona, scattered light, stars to 12th magnitude, four planets (Venus, Jupiter, Mercury and Mars), the instrumental PSF, cosmic rays, the non-shutter read-out effect, noise, saturation and blooming and a dummy CME.*

## 6. Exposure Sequences and Image Subtraction

To extract the CME signal we must accumulate exposures, to ensure that the CME intensity becomes significantly brighter than the noise level. The code allows the user to select the number of images in the sequence. As mentioned above, we do this by summing a series of exposures and cleaning each of cosmic rays, on board, prior to summing. If this is not done we would anticipate over 25% of the pixels being contaminated by cosmic ray hits in the final image of any sequence.

The nominal image sequences for HI-1 and HI-2 are 70 and 60 exposures of 12 s and 60 s, respectively. This should provide adequate statistical accuracy. Very roughly, taking estimates from the plots given above, if we assume an F-coronal contribution of about 170 photons/pixel/sec, a single exposure would give 10200 ph/pixel for HI-2, with an anticipated error of order 1300. The anticipated CME

signal is of order 34 (see below), i.e. readily swamped by noise. However, for a total (accumulated) exposure time of 3600 s (60 x 60 s), the anticipated count rate would be of order 61200 photons with an error of 780, compared to a CME signal of over 2000 photons.

Once a summed image has been completed and returned, the CME signal is identified either by the subtraction of a base-frame or the subtraction of a recent image. The former technique is illustrated below. First, we note that for LASCO/SOHO a base-frame is generated using a month of images. The minimum value for a pixel location during that month is declared to be the background corona plus stray light. Clearly stars move in that time and are not extracted.

A 60 exposure-summed image of 60 s each (total 3600 s exposure time) for HI-2 has been created using the methods described above. For such a period, we can construct a base-frame from knowledge of the F-coronal intensity distribution and the stellar positions and intensities. This estimated base-frame can include an estimate of blooming and saturation but it cannot include the noise contribution. It can include the planets. It can also include the non-shutter gradient estimated from the known intensities. In theory the only unknown is the noise - if the cosmic rays are removed effectively. The base-frame for this particular study is shown in Fig. 6.1.

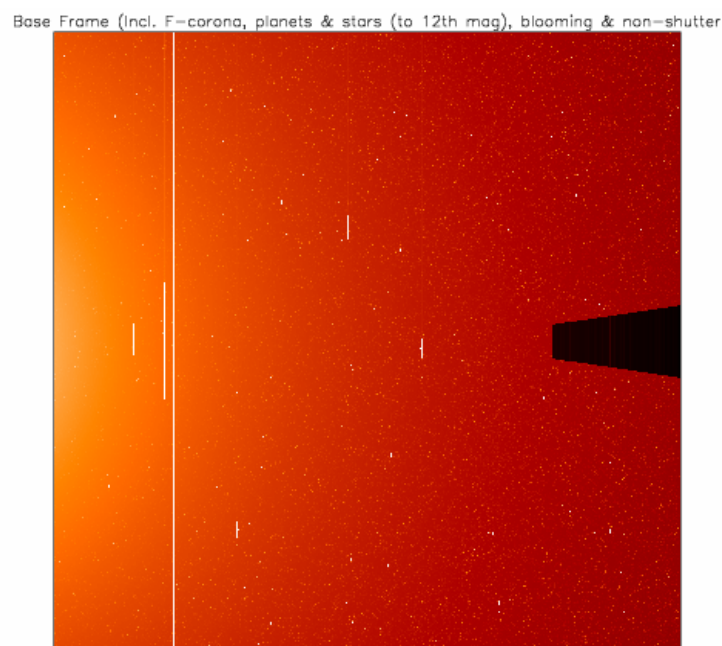


*Fig. 6.1: The estimated base-frame for a 60-exposure 60 s HI-2 sequence*

The base frame is subtracted from the simulated image and the final product, in this case is shown in Fig. 6.2.

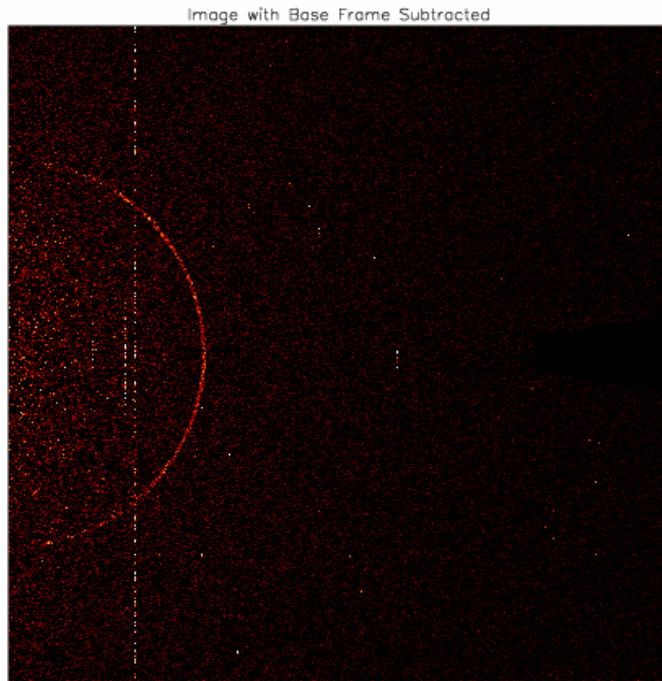


Fig. 6.2: The final image - the 60-exposure 60 s HI -2 sequence with the calculated base-frame subtracted. The CME loop is clear.

If the base-frame is accurate, and the cosmic rays extracted efficiently, Fig. 6.2 should only include the contribution from noise and the CME. Given the accumulated exposure time, the CME intensity should be clear.

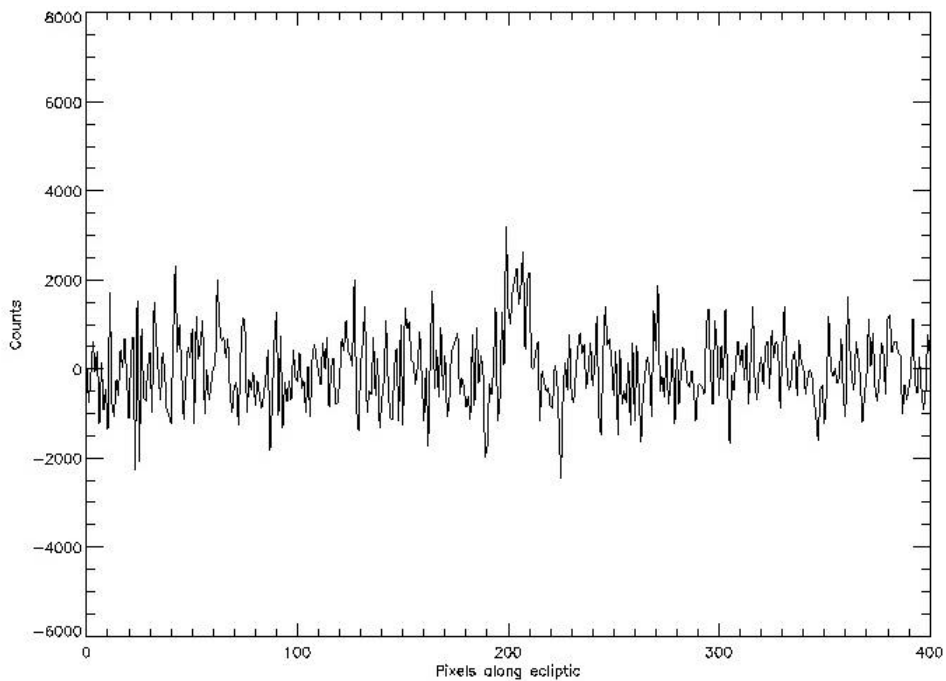


Fig. 6.3: A plot of intensity vs pixel along the ecliptic line, from pixel 400 to 800, from the image of Fig. 6.2. The CME can be seen centred on pixel 200.

The extraction of the CME above the noise level seems to be perfectly achievable. However, this has assumed that we can construct a good base-frame and that we can extract cosmic rays. However, we are extracting the stellar intensities, unlike LASCO/SOHO. The model calculations have assumed that we know where all stars are located and we can subtract them - down to 12<sup>th</sup> magnitude - including the PSF distributions. To put this into perspective, there are 221,4141 magnitude 12 stars in the HI-2 field of view, which, for a 60 s exposure provide an intensity of 1,722 counts (i.e. 28.7 x 60) each. If we consider an arbitrary pixel, located at (605,1024), this compares to an F-coronal intensity (including stray light) of 10,654 counts. Thus, some 5% of the HI-2 pixels are centred on a 12<sup>th</sup> magnitude star providing an intensity departure some 16 times the anticipated noise level on the F-coronal intensity. Here, we are considering a single exposure. If we sum exposures, we do bring the relative noise levels down, but we do not reduce the intensity of the stars. In effect, we are banking on being able to extract the stars effectively. We cannot increase the accumulated exposures for the CME intensity to exceed the intensity of the background stars!

In effect, stellar intensities are spread according to the PSF. Thus, we are looking at the peak intensities (12 magnitude) at 6 times the anticipated noise level. However, the PSF also dictates that more pixels are included. As a rough guide, if we consider that the bulk of the stellar intensity is contained within 9 pixels (90%), then over 45% of the HI-2 pixels are seeing some light from 12<sup>th</sup> magnitude stars.

Thus, whereas the cosmic ray cleaning process must be efficient, and the noise levels must be kept to a minimum, by far the most challenging aspect is the extraction of the CME data from within the stellar 'noise'. To do this we must consider the following image handling procedures:

- (i) Model Base Frame Subtraction: Construct a model base-frame, which contains the anticipated F-corona and all known stellar and planetary locations/intensities, including saturation effects and the non-shutter read out. The base-frame will vary with time, as the stars move.
- (ii) Empirical Base Frame Subtraction: Produce a regular base-frame (semi-automatically) using HI image data, by comparisons of images and 'fixed' features and intensities.
- (iii) Image-Image Subtraction: Ignore the stellar background etc... and simply subtract adjacent images or recent (pre-event) images to identify the CME activity.

Item (i) may be impossible! However, we may wish to consider its feasibility.

Item (ii) could be done in a semi-automatic way by comparison of images on a regular basis. A rolling average intensity approach could be used. We must

extract stars, so the 'minimum' intensity approach over a month is not applicable. It is more likely to be rolling over a much shorter period.

Item (iii) is workable and is probably the simplest and most crude approach.

In effect, what we have done above is item (i).

It is worth noting that different processing/differencing techniques should be considered for different targets. These are summarised in the table. Thus, all methods should be available.

HI Target	Detection Methods to Consider
CME	Base Frame Subtraction (Model or Empirical) or image-image subtraction.
Comet/NEO	Image-image subtraction or empirical base-frame subtraction
Streamers/structure in the heliosphere	Model Base Frame Subtraction or image-image subtraction
Planets	Raw images

The other feature which is evident from the HI images is the occasional 'stripe' caused by the non-shutter operation extending from a stellar or planetary source to the upper edge of the image.

How many stars will show a stripe of this kind, which is of concern to us? We require the stripe intensity to be less than that of the CME intensity. For HI-1 and HI-2 we take CME intensities of order  $10^{-13}$  Bo and  $10^{-15}$  Bo. With a solar intensity, Bo, of  $10^{17}$  ph/s (spread over 2076 and 176 pixels for HI-1 and HI-2), this gives 58 and 34 ph/pixel for the nominal 12 s and 60 HI-1 and HI-2 exposures, respectively.

The line transfer 'exposure times' are 2048  $\mu$ s. Section 3.2 shows the intensities of different stellar magnitudes. For HI-1 and HI-2, we are concerned about stars (or other objects) with intensity greater than  $(58 / 2048 \times 10^{-6})$  and  $(34 / 2048 \times 10^{-6})$  ph/s, i.e. 28,320 and 16,602 ph/sec. However, the PSF dictates that <40% of the intensity will appear in the core pixel, so this means that our concern is for stars of intensity greater than 70,800 and 41,505 ph/s. This translates to stars >3rd magnitude for HI-1 and >4th magnitude for HI-2. This is well under 10 sources for HI-1 and 70 for HI-2, i.e. it can potentially influence up to 3.4% of the 2048 columns. However, this is a known effect and can be extracted through knowledge of the stellar source distributions and intensities or by recent frame subtraction. It also influences only those columns containing the stars/planets and, thus, can be ignored with little effect on the scientific investigation.

## 7. The IDL Code and the Next Steps

The original HI\_SIM code was written in IDL. Its lack of sophistication is a reflection of the limitations of the author as well as the fact that his IDL experience runs back to the Solar Maximum Mission days and probably includes some rather old fashioned routines! It has recently undergone several re-workings in order to optimise the code and to add extra features. It now runs in a fraction of the time it once took (a few minutes rather than a few hours!) and is able to mimic the anticipated intensity contributions for the HI instruments. The code is freely available to anyone and it is well annotated for ease of understanding.

The current version (Version 3.4) is able to model the HI-1 and HI-2 images, for any given exposure time, including contributions from the F-corona, the planets and the stars to 12th magnitude, and includes stray light, the point spread function, noise, saturation and blooming. It also includes the non-shutter effects. It includes cosmic rays and a model CME. New to this version is the addition of cosmic ray tracks (rather than point sources), the inclusion of the occulter in HI 2 images, a few bug fixes and a significant amount of optimisation.

The simulation raises and confirms a number of issues. From the point of view of the on-board and ground software for SECCHI, we must have or consider the following procedures:

- The ability to return the entire square CCD image for either HI-1 or HI-2 (not just the circular areas previously defined) or any sub-image, as pre-selected.
- The ability to calculate a model base-frame using knowledge of the F-corona, stars and planets, which can be used to subtract non-CME intensities from the HI images. This base frame will change with time, and must include estimated effects of saturation and blooming, the PSF, and the non-shutter effects.
- The ability to construct an empirical base-frame using recent data on a regular and, probably, semi-automatic basis.
- The ability to make image-image subtractions for any selected image pair.
- The ability to extract cosmic rays effectively, on board, prior to image summing. (We ought to be able to disable this as well, to make cosmic ray investigations on occasions).

Many of the intensities used here are extreme - e.g. the brightest stars are assumed to be in the HI fields of view, the four planets are modelled using their maximum magnitudes, and we only use the equatorial F-coronal values. A

relaxation of any of these is beneficial for the analysis of images for CME research.

Finally, there are some instrumental assumptions. The final baffle performance may well exceed that used here. The detector performance with regard to blooming needs to be tested.

The next planned steps are the following:

(i) Produce a series of HI-1 and HI-2 images, which include all effects (including cosmic rays and a CME) for use in the development of cosmic ray cleaning procedures and in the development of differencing methods for CME analysis. These are to be co-ordinated between Davis (RAL) and Wang (NRL).

(ii) Investigate further methods for non-shutter correction/extraction (Davis, RAL).

(iii) Run the HI\_SIM code as a flexible tool for the investigation of different scientific operations, for a variety of targets (CMEs, comets, planets, NEOs etc...).

Further versions of this document will report on progress in these areas.

*[File HI\_SIM\_document\_version3.doc 08/08/2003]*